# Novel application for pseudopodia proteomics using excimer laser ablation and two-dimensional difference gel electrophoresis

Akihiko Ito[1,2,7], Takahiro Mimae[2,3,7], Ying-Shan-Zhu Yamamoto[4], Man Hagiyama[1,2], Jun Nakanishi[5], Masaoki Ito[3], Yoichiroh Hosokawa[6], Morihito Okada[3], Yoshinori Murakami[2] and Tadashi Kondo[4]

We developed a novel application to conduct pseudopodia proteomics. Pseudopodia are ventral actin-rich protrusions and play functional roles in cell migrations. Identification of pseudopodia proteins leads to a further understanding of malignant phenotypes of tumor cells and novel therapeutic strategies. In our application, tumor cells were placed on a fibronectin-coated porous membrane to form pseudopodia. According to the motile potentials of the cells, the cells formed pseudopodial microprocesses in the pores. An excimer laser, which was used for ophthalmic refractive surgeries, horizontally ablated cells at the membrane surface to remove the cell body. The microscopic observations and the protein expression studies suggested that the laser treatment caused no apparent damages to pseudopodia. Proteins in whole cells and pseudopodia fractions were individually solubilized, labeled with a highly sensitive fluorescent dye, and separated using two-dimensional difference gel electrophoresis. Among 2508 protein spots observed, 211 had different intensity between whole cells and pseudopodia fractions (more than fourfold differences and $P$-value of $<0.05$). The protein enrichment depended on the pore size. Mass spectrometric protein identification revealed 46 pseudopodia-localizing proteins. The localization of novel pseudopodia-localizing proteins such as RAB1A, HSP90B, TDRD7, and vimentin was confirmed using immunohistochemical examinations. The previous studies demonstrated that these four proteins may function in the cell migration process. This method will provide insights into the molecular details of pseudopodia and a further understanding of malignant phenotypes of tumor cells and novel therapeutic strategies.
*Laboratory Investigation* (2012) **92**, 1374–1385; doi:10.1038/labinvest.2012.98; published online 2 July 2012

Polarized formation of pseudopodial protrusion during cell migration plays a central role in a variety of physiological and pathological processes, including embryo development, wounding healing, immunity, and cancer metastasis.[1,2] An *in vitro* model system was established to recover pseudopodia from cell bodies in order to identify signal pathways and proteins mediating cell migration.[3] In the model system, cells are plated on a porous membrane and allowed to extend pseudopodia through the pores to the ventral side of the membrane in a chemoattractant-dependent manner. To isolate the pseudopodia, the cell bodies are wiped off from the top of the membrane using a cotton-tipped swab, and

proteins are extracted from the resultant membrane. Previously, mass spectrometry-based proteomics combined with this approach were used to identify numerous proteins in pseudopodia protrusions.[4–6] However, there were critical limitations to the method used in the previous report. Manual separation of pseudopodia from cell bodies created the potential for contamination of cell body components into the pseudopodial extract. Thus, a novel application to purify pseudopodia from cell bodies may provide more precise results. Additionally, the mass spectrometry-based approach described in the previous report did not allow for quantitative comparison between the cell body and pseudopodia, and

[1]Department of Pathology, Faculty of Medicine, Kinki University, Osaka, Japan; [2]Division of Molecular Pathology, Department of Cancer Biology, Institute of Medical Science, University of Tokyo, Tokyo, Japan; [3]Department of Surgical Oncology, Research Institute for Radiation Biology and Medicine, Hiroshima University, Hiroshima, Japan; [4]Division of Pharmacoproteomics, National Cancer Center Research Institute, Tokyo, Japan; [5]Nidek, Gamagori, Aichi, Japan and [6]Nara Institute of Science and Technology, Ikoma, Nara, Japan
Correspondence: Dr T Kondo, MD, PhD, Division of Pharmacoproteomics, National Cancer Center Research Institute, 5-1-1 Tsukiji, Chuo-ku, Tokyo 104-0045, Japan.
E-mail: takondo@ncc.go.jp
[7]These authors contributed equally to this work.

a highly sensitive and quantitative proteomics system is necessary.

We hypothesized that an excimer laser-assisted cell etching technique was a possible remedy for removing cell bodies, avoiding damages on the pseudopodia components. This technique is widely used in clinics as a tool for ophthalmic refractive surgeries such as laser-assisted in situ keratomileusis (LASIK). In LASIK, after the epithelium is flapped from Bowman's layer, the superficial anterior corneal tissue is reshaped by a topographically assisted excimer laser to improve myopia, hypermetropia, and astigmatism.[7] Because the excimer laser ablates living tissues in a precisely horizontal manner without causing thermal damage to the surrounding area, complications rarely occur.[8] We hypothesized that by adjusting the laser ablation front to the ventral membrane surface of the cells, the cell body could be ablated while the protrusion in the pores remain intact.

Recent advent proteomics technologies have enabled global protein expression profiling.[9] Using novel ultrahigh sensitive fluorescent dyes, gel-based protein expression studies have allowed quantitative expression profiling for a small number of cells such as those recovered by laser microdissection.[10–13] The use of multiple fluorescent dyes with different emission and excitation wavelengths for protein labeling allows inclusion of internal controls in large format gels so that highly reproducible results are expected using two-dimensional difference gel electrophoresis (2D-DIGE). We developed a proteomics system using these methods with a highly sensitive fluorescent dye and a large format gel apparatus.[10,11] We challenged biomarker development and target discovery using 2D-DIGE.[14]

In this study, we applied a combination of an excimer laser-assisted cell etching technique and 2D-DIGE to characterize proteins in pseudopodia. We identified proteins unique to pseudopodia and confirmed their localization by immunohistochemical examinations.

## MATERIALS AND METHODS
### Cell Culture Conditions
MDA-MB-231 human breast cancer cells, B16-F10 murine melanoma cells, murine NIH3T3 fibroblast cells, and A549 human lung adenocarcinoma cells were purchased from American Type Culture Collection (ATCC, Rockville, MD, USA). MDA-MB-231 was maintained in L-15 (Sigma-Aldrich, Gillingham, UK) supplemented with 10% FBS, 100 units/ml penicillin, 100 $\mu$g/ml streptomycin (Invitrogen, Carlsbad, CA, USA), and 0.3 g/l L-glutamine (Sigma-Aldrich). B16-F10, NIH3T3, and A549 were grown in Dulbecco's modified Eagle's medium (DMEM) (NakalaiTesque, Kyoto, Japan) supplemented with 100 units/ml penicillin, 100 $\mu$g/ml streptomycin (Invitrogen), 10 and 5% FBS, respectively. MDA-MB-231 cells were maintained at 37 °C in air and B16-F10, NIH3T3, and A549 cells were maintained in a 5% $CO_2$ incubator.

### Preparation of Conditioned Medium
When NIH3T3 cells reached confluence, the medium was replaced with FBS-free DMEM and the cells were maintained for an additional 3 days. Next, the culture medium was filtrated and stored as conditioned medium at −80 °C.

### Cell Culture on Porous Membrane
Polyethylene terephthalate (PET) membranes (BD, Franklin Lakes, NJ, USA) with pore size of 1 or 3 $\mu$m were coated with 1 $\mu$g/ml fibronectin (Sigma-Aldrich) in Dulbecco's phosphate-buffered saline (D-PBS)[15] for 30 min. After removing the fibronectin-containing D-PBS, the membrane was bottomed with a 1:1 ratio of culture medium and the above-mentioned NIH3T3-conditioned medium and the culture medium was added to the membrane.[6] Next, 1 × 10^{5} of MDA-MB-231 cells, 1 × 10^{4} of B16-F10 cells, and 1 × 10^{5} of NIH3T3 cells/well were seeded in 12-well culture plate and cultured on the membrane for 2 days at 37 °C in a 5% $CO_2$ incubator.

### Microscopic Observations
After 2 days of culture on the fibronectin-coated porous PET membrane, MDA-MB-231 and B16-F10 cells on the PET membrane were washed with PBS, fixed with 4% formalin, embedded in paraffin, and cut into sections using an SM2000R (Leica Microsystems, Wetzlar, Germany). Sections were stained using hematoxylin–eosin (HE) and observed using a light microscope (BX51, Olympus, Tokyo, Japan) equipped with a CCD camera DP72 (Olympus).

### Excimer Laser Ablation and Protein Extraction
An MDA-MB-231 cell culture membrane was placed on an irradiation stage of a keratectomy system assisted by an argon fluoride excimer laser (193 nm, 10 Hz; EC-5000 CXIII, Nidek, Gamagori, Japan) adjusted for phototherapeutic keratectomy.[16,17] Laser scanning was achieved on the membrane substrate by using an image rotator mirror and exposed homogeneously on the area with a diameter of 8 mm. Laser pulse energy was adjusted to be 14 mJ, and 12 pulses were shot per scan. The laser scanning process was monitored using a CCD camera with oblique illumination. Laser scanning was manually continued until disappearing of the light scattering due to the cell bodies. To determine the scanning number, the irradiated cells and membrane were stained using HE after formalin fixation and were observed using a light microscope after mounting to examine whether the cell bodies were completely removed. The cell bodies were perfectly extracted with a scanning number of approximately 20 (range between 18 and 24). We serially processed 100 culture membrane samples. Immediately after each irradiation, the processed area of the membrane was cut using a hollow leather punch with a diameter of 5 mm and frozen in liquid nitrogen.

Protein extraction was performed from the pool of 100 frozen membranes. Briefly, the membranes were macerated,

and each protrusion lysate was prepared using lysis buffer containing 50 mM Tris-HCl (pH 7.4), 150 mM NaCl, 1% Triton X-100, 20 mM EDTA, and a protease inhibitor mixture by rotating at 4 °C. For the whole-cell lysate, 2-day cultures of MDA-MB-231 on the porous membrane were scraped, and the scraped fractions were extracted using lysis buffer. After centrifugation at 13 000 r.p.m. for 5 min at 4 °C to remove insoluble material, the supernatant was recovered and used in subsequent protein expression studies.

A schematic diagram of laser ablation and protein extraction is provided in Figure 1. The video image of laser ablation is available in Supplementary Video Data.

## Immunoblotting and Silver Staining

Protein lysates from human lung tissues (P1234156 and P1234159) were purchased from BioChain Institute (Hayward, CA, USA). Protein lysates from MDA-MB-231 cells and A549 cells and human lung tissue were suspended in SDS-PAGE sample buffer containing 2% SDS, 50 mM dithiothreitol, 50 mM Tris, and 10% glycerol, and incubated at 95 °C for 5 min. The proteins were fractionated using SDS-PAGE and a 10% polyacrylamide gel. Fractionated proteins were transferred onto a polyvinylidene difluoride membrane (Millipore, Bedford, MA, USA), blocked with 5% skim milk for 30 min, and reacted with an antibody against integrin $\alpha 2$ (2/CD49b,
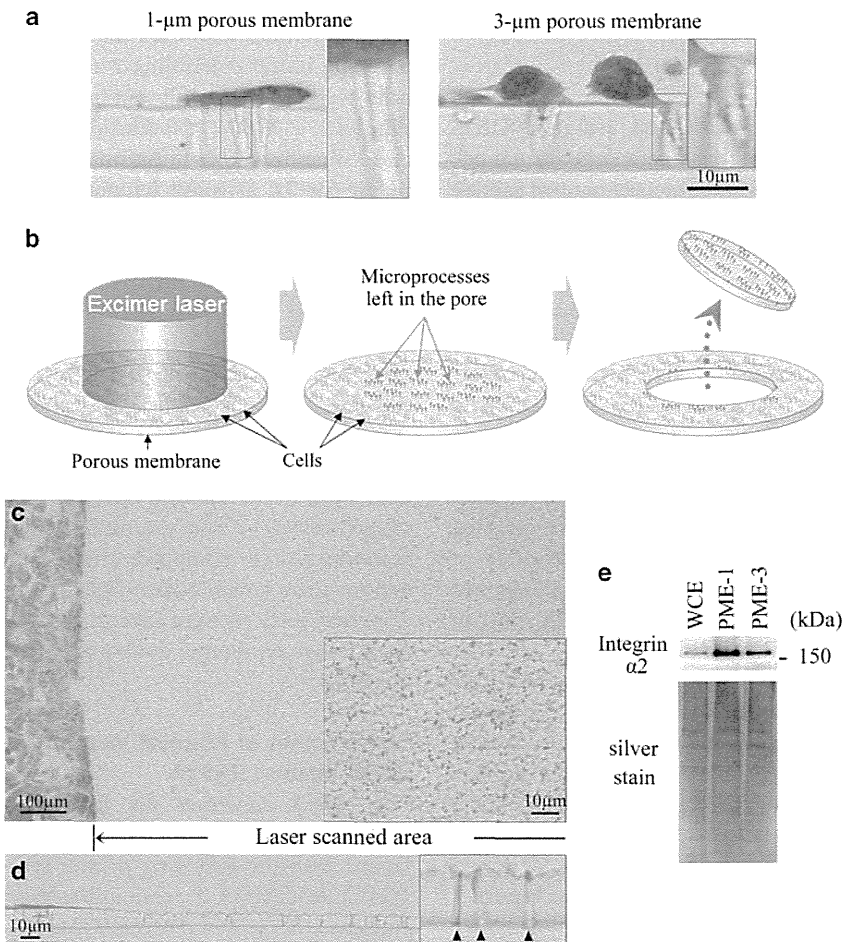


**Figure 1** Microscopic observation of pseudopodia in the porous membrane. Pseudopodia in pores with diameters of 1 $\mu$m (**a**, left) or 3 $\mu$m (**a**, right). Enlarged image in the box shows pseudopodial microprocesses. A schematic diagram of excimer laser ablation is shown. The laser scanning plane was adjusted to the surface of the porous membrane (**b**, left). The pulse energy and scanning cycles were optimized to completely remove cell bodies and leave the remaining microprocesses intact in the membrane pores (**b**, middle). Membranes were punched out after ablation and frozen in liquid nitrogen (**b**, right). The membrane stained with hematoxylin–eosin (HE) was ablated, and no cell bodies remained in the ablated area. The boxed area shows the dot-like appearance of the remaining pseudopodial microprocesses (**c**). Vertical images of the whole cell and pseudopodia after laser ablation. Arrows in the box indicate pseudopodia of higher magnitude. Enlarged image in the box shows that pseudopodial microprocesses stained with HE remained intact after laser ablation (**d**). Protein extracts from 1 and 3 $\mu$m porous membranes were defined as pseudopodial microprocess extracts PME-1 and PME-3, respectively, and the whole-cell extract as WCE. Western blotting revealed highly enriched integrin $\alpha 2$ in PME-1 and PME-3 compared with WCE. A gel prepared in parallel was silver-stained to control for protein loading (**e**).

BD, 1:1000 dilution), RAB1A (C-19, Santa Cruz Bio-technology, Santa Cruz, CA, USA, 1:100 dilution), TDRD7 (HPA024529, Sigma-Aldrich, 1:100 dilution), HSP90B (HPA003901, Sigma-Aldrich, 1:100 dilution), and $\beta$-actin (AC-15, Sigma-Aldrich, 1:100 dilution) at 4 °C overnight. Then, the membranes were incubated with horseradish peroxidase-conjugated secondary anti-mouse antibody (Santa Cruz Biotechnology, 1:1000 dilution) for integrin $\alpha$2 and $\beta$-actin and anti-rabbit antibody (Santa Cruz Bio-technology) for RAB1A, TDRD7, and HSP90B at 4 °C for 2 h. Protein complexes were detected using ECL Western Blotting Detection Reagents (GE Healthcare, Uppsala, Sweden). The proteins fractionated by SDS-PAGE in parallel experiments were silver-stained using the Proteo Silver™ Plus Silver Stain Kit according to the manufacture's instruction (Sigma-Aldrich).

## 2D-DIGE and Protein Identification by Mass Spectrometry

Protein expression profiling was achieved using 2D-DIGE with a highly sensitive fluorescent dye and a large format gel, as previously described.[10] Briefly, the internal control sample was prepared by mixing a portion of all individual samples. Next, 5 $\mu$g of the internal control sample and individual sample were labeled with Cy3 and Cy5 (CyDye DIGE Fluor saturation dye; GE Healthcare), respectively, according to our previous report.[10] These differentially labeled protein samples were mixed and separated using 2D-DIGE. The first-dimension separation was achieved using IPG DryStrip gels (24 cm in length; pI, 4–7, GE). The second-dimension separation was achieved using SDS-PAGE with a large format gel apparatus (33 cm separation distance; Biocraft, Itabashi, Tokyo, Japan). After electrophoresis, the gels were scanned using laser scanners (Typhoon Trio, GE Healthcare) at appropriate wavelengths. The intensity of the Cy5 image was normalized to that of the Cy3 image for all protein spots in the identical gel using the Progenesis SameSpot software (Nonlinear Dynamics, Newcastle upon Tyne, UK). All samples were analyzed in triplicate, and the intensity between the three gels was normalized for statistical analysis. System reproducibility was verified by comparing protein profiles obtained from three independent separations of identical samples.

Proteins corresponding to the protein spots were identified using mass spectrometry according to our previous report.[10] Briefly, MDA-MB-231 cells were treated with urea lysis buffer (6 mol/l urea, 2 mol/l thiourea, 3% CHAPS, 1% Triton X-100), and total cell lysate was recovered after centrifugation. Next, 100 $\mu$g of protein was separated using two-dimensional gel electrophoresis as described above, and target protein spots were recovered as gel plugs by using a protein spot recover machine (Molecular Hunter, AsOne, Osaka, Japan). Proteins in the gel plugs were manually digested using modified trypsin (Promega, Madison, WI, USA), and the trypsin digests were subjected to LC/MS

(Finnigan LTQ linear ion trap mass spectrometer, Thermo Electron, San Jose, CA, USA). The Mascot search (version 2.1; Matrix Science, London, UK) was conducted to identify the mass of the peptide ion peaks compared with the SWISS PROT database (Homo sapiens, 12 867 sequences in the Sprot_47.8 FASTA file). Proteins with Mascot scores of ≥ 33 with at least 2 peptides were considered as positively identified.

## Immunostaining and Confocal Microscopy

A total of $5 \times 10^4$ MDA-MB-231 cells were cultured on fibronectin-coated porous membrane for 2 days. The cells were washed 3 times with PBS and fixed with 4% formalin at room temperature for 15 min. Membranes were washed 3 times with PBS and permeabilized with 0.25% Triton-X (Sigma-Aldrich) in PBS at room temperature for 5 min. After washing 3 times with PBS, the membranes were incubated in blocking buffer containing 2% BSA in PBS for 10 min. The cells were treated with antibodies against RAB1A (1:12.5 dilution), TDRD7 (1:50 dilution), HSP90B (1:1000 dilution), and vimentin (1:100 dilution) (RV20, BD) in the blocking buffer for 2 h at room temperature. Subsequently, the cells were incubated with Alexa Flour 488–conjugated goat anti-rabbit IgG antibodies (1:100 dilution) (Molecular Probes, Invitrogen) against RAB1A, TDRD7, and HSP90B, and Alexa Flour 488–conjugated goat anti-mouse IgG antibody (Molecular Probes, Invitrogen, 1:100 dilution) against vimentin antibody in the blocking buffer for 1 h at RT. After washing 3 times with PBS, phalloidin (Sigma-Aldrich) staining was performed for 20 min at room temperature. Next, the stained cells on the membrane were washed 3 times with PBS, mounted, and covered with glass coverslips. The stained cells were then examined using a NIKON A1 confocal scanning system equipped with 488-nm argon and 568-nm helium-neon lasers (Nikon Corporation, Tokyo, Japan). X-Y-Z vertical sections were generated using a 0.5-$\mu$m motor step. Each image represents double averaged (40- to 50-line scan) images.

## Construction of Plasmid Vectors Expressing RAB1A and siRNA against RAB1A

The cDNA construct for RAB1A inserts was amplified by PCR using KOD FX DNA polymerase (Toyobo, Osaka, Japan) with the following primer set: sense, 5'-CAGTGACA TGTCCAGCATGA-3' (containing the first codon of RAB1A); antisense, 5'-GCAGCTACATACAGTACAATTCAGG-3' (containing the stop codon of RAB1A). The PCR products were resolved by electrophoresis on 1% agarose gels and stained with ethidium bromide. Targeted bands were excised from gels and DNA was extracted and purified using the Wizard® SV Gel and PCR Clean-Up System (Promega) as described by the manufacturer. Extracted DNA was incubated at 70 °C with Taq polymerase and adenosine triphosphate for 30 min and ligated into pTA2 vector (Toyobo). Then, pTA2-RAB1A was enzymatically restricted with BamHI and EcoRV. The

restricted pTA2-RAB1A was resolved by electrophoresis on 1% agarose gels and stained with ethidium bromide. Targeted bands were excised from gels and DNA was extracted and purified using the Wizard SV Gel and PCR Clean-Up System. Extracted DNA chains were annealed and ligated into the BamHI/HpaI sites of pCX4-bsr, a modified pCXbsr retroviral vector[18] provided by Dr T Akagi (Osaka Bioscience Institute, Osaka, Japan), and sequenced. The plasmids were extracted and the accuracy of the constructs was confirmed by sequencing.

The pSilencer4.1-CMVneo siRNA plasmid vector (Ambion, Austin, TX, USA) was used to construct pSilencer4.1-CMVneo-si-RAB1A and pSilencer4.1-CMVneo-scramble. A DNA chain with the RAB1A-targetting siRNA sequence or the scrambled fragment one was purchased from Ambion. The RAB1A-targetting sequences were as follows: 5'-GATCCCA ATCACCTCCAGTTATTATTCAAGAGATAATAACTGGAGGT GATTGTT-3' (sense) and 5'-AGCTTAACAATCACCTCCAGT TATTATCTCTTGAATAATAACTGGAGGTGATTGG-3' (anti-sense). The sequences had no homology with any other predicted protein-coding genes of the human genome according to manufacturer's instruction. The DNA chains were annealed and ligated into the BamHI/HindIII sites of pSilencer4.1-CMVneo to generate pSilencer4.1-CMVneo-si-RAB1A. The negative control pSilencer4.1-CMVneo-scramble vector was constructed in the same manner. The plasmids were extracted and the accuracy of the insert sequence was confirmed by sequencing.

## Transfection and Measurement of the Pseudopodial Length

For overexpression experiments, MDA-MB-231 cells on fibronectin-coated 3 μm porous membrane with NIH3T3-conditioned medium were transiently transfected with pCX4-bsr-RAB1A using FuGENE® 6 (Roche Applied Science, Indianapolis, IN, USA). In brief, $2.0 \times 10^5$ cells were seeded on 60 mm culture dishes overnight until 50–80% confluence was reached. Serum-free medium (194 μl) and 6.0 μl of FuGENE 6 reagent were mixed in 1.5 ml tubes and incubated for 5 min at room temperature. Plasmid vectors (2.0 μg each) were added and the contents were mixed and incubated with transfection reagent and DNA complex for at least 15 min at room temperature. The transfection reagent and DNA complex were added dropwise to the cultured cells and incubated for 48 h. For knockdown experiments, MDA-MB-231 cells were transfected transiently with the pSilencer4.1-CMVneo-si-RAB1A and scramble-pSilencer4.1-CMVneo vector constructs using Nucleofector with solution V (Lonza, Basel, Switzerland).

Then, the cells were immunostained with phalloidin and applied to confocal microscopy.

## Statistical Analysis

Data about the length of the pseudopodial microprocesses were analyzed using Student's t-test and box plot method. A P-value of ≤0.05 was regarded as significant.

# RESULTS

## Pseudopodial Microprocesses in Porous Membranes

MDA-MB-231 breast cancer cells were seeded onto 10 μm thick membranes with 1 or 3 μm pores. We found that membrane protrusions (eg, pseudopodia) were extended into the membrane pores from the ventral side of the cell body (Figure 1a). Protrusion diameters were <10 nm and 1 μm in 1-μm (Figure 1a, left) and 3-μm (Figure 1a, right) porous membranes, respectively. Protrusion lengths varied from 2 to 10 μm in both types of porous membranes (Figure 1). Formation of membrane protrusions did not occur in the absence of NIH3T3-conditioned medium, although it was detectable when cells were cultured on 8 μm porous membrane (data not shown). Highly invasive melanoma cells, B16-F10 cells, formed similar membrane protrusions in the same tissue culture conditions as MDA-MB-231; however, nontumorigenic cells such as NIH3T3 did not (data not shown).

## Isolation of Pseudopodial Microprocesses

An excimer laser-assisted cell etching technique was used to remove cell bodies from the porous membrane. A schematic diagram of the laser ablation is illustrated in Figure 1b and the video image of the laser ablation process is available in Supplementary Video Data. The video image showed that the cell body was removed in a short period. After treatment with an excimer laser-assisted cell etching, the membrane protrusions were observed to be dot-like structures (Figure 1c). Vertical images showed that cell bodies were completely removed and pseudopodia structures remained intact by visual inspection (Figure 1d). We examined the contents of integrin α2 that had accumulated in epithelial cell pseudopodia.[19] Immunoblotting also revealed that integrin α2 was highly enriched in the pseudopodia fraction compared with the whole cell, regardless of pore diameter, and without degradations (Figure 1e). In addition, enriched localization of integrin α2 was observed in pseudopodia on confocal imaging (Supplementary Figure S1).

## Proteins Enriched in Pseudopodial Microprocess Extract

We compared protein content in pseudopodial microprocess extract (PME) and whole-cell extract (WCE) using 2D-DIGE and an internal control sample (Figure 2a). Proteome data resulting from 2D-DIGE included 2508 protein spots (Figure 2b and Supplementary Figure S2a). Scatter plot analysis demonstrated that high reproducibility was observed by performing the experiment in triplicate; the intensity of at least 97.2% protein spots was scattered within twofold differences (Supplementary Figure S2b). When identical samples were independently separated 3 times, the standardized and averaged intensity of at least 97.2% protein spots scattered within a twofold difference (Supplementary Figure S2b). Thus, the protein spots that met the following criteria were subjected to mass spectrometric protein identification: spots for the 1 μm porous membrane group, a false
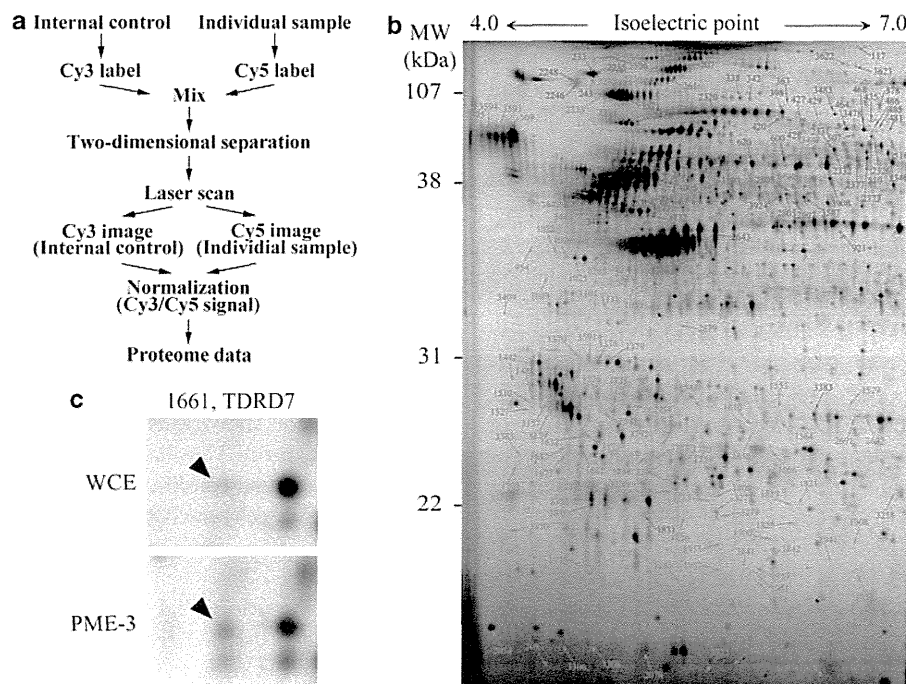
**Figure 2** Protein expression profiling by two-dimensional difference gel electrophoresis (2D-DIGE). Schematic diagram of work flow of 2D-DIGE (a). Image of separated proteins on the gel. Enlarged 2D image is shown in Supplementary Figure 1A (b). The location of protein spots for TDRD7 was observed in pseudopodia (upper) and whole-cell (lower) lysates (c).

discovery rate of <0.001, and a fold difference of >6 between the protrusions and the whole cell group; spots for 3 μm pore membrane group, a false discovery rate of <0.001, and a fold difference of >4 between the protrusions of the 3 μm porous membrane group and the whole cell group. According to these criteria, we selected 67 and 132 spots with higher intensity and 29 and 74 spots with lower intensity in PME for the 1 μm porous membrane (PME-1) and PME for the 3 μm porous membrane (PME-3) than in WCE, respectively (Table 1). Protein identification using liquid chromatography-mass spectrometry/mass spectrometry (LC-MS/MS) revealed 21 and 45 unique proteins with higher expression in PME-1 and PME-3 than in the WCE, and 19 and 36 proteins with lower expression in PME-1 and PME-3, respectively (Table 1, Supplementary Tables S1–S3; all supportive data for protein identification, including raw data, are available upon request). The representative mass spectrum is shown in Supplementary Figure S3. All but two proteins were commonly enriched or lowered in PME-1 and PME-3. As an example of proteins in the pseudopodia fraction, the localization of TDRD7 (spot number 1661) is demonstrated in Figure 2c.

### Subcellular Localization of Identified Proteins

Localization of the identified proteins was immunohistochemically validated using antibodies against RAB1A,

HSP90B, TDRD7, and vimentin. First, we examined subcellular localization of these proteins in MDA-MB-231 cells without treatment using NIH3T3-conditioned medium. The four proteins showed unique localizations: RAB1A, diffuse pattern in the nucleus and cytoplasm (Figure 3); HSP90B, mesh-like or punctate appearance in the cytoplasm; TDRD7, spotty features in the nucleus; and vimentin, cytoskeletal fibrous structures (Figures 4–6, respectively). Phalloidin staining demonstrated well-developed actin stress fibers across cells. No pseudopodial microprocesses were observed when NIH3T3-conditioned medium was not used. After treatment with NIH3T3-conditioned medium, pseudopodial microprocesses were observed and these proteins localized in pseudopodial microprocesses with actin stress fibers at the cell-membrane interface. Immunohistochemical analysis confirmed a novel localization of RAB1A, HSP90B, TDRD7, and vimentin in pseudopodial microprocesses, which is consistent with the results of 2D-DIGE (Table 1 and Figures 3–6). In addition, endogenous RAB1A, HSP90B, TDRD7, and vimentin expression for naive MDA-MB-231 cells, human lung tissue, and human lung adenocarcinoma A549 cells was validated using western blot (Supplementary Figure S4).

### The Length of Pseudopodial Microprocesses

To validate whether the identified molecules are involved in forming pseudopodial microprocesses, RAB1A over-

## Table 1 Proteins upregulated in pseudopodia microprocesses in 1 or 3 μm porous membrane

| Accession no. | Identified protein[a] |
| --- | --- |
| *Cytoskeleton (3)* | |
| Actin-associated (2) | |
| P60709 | Actin, cytoplasmic 1 |
| P04632 | Calpain small subunit 1 |
| *Intermediate filament (1)* | |
| P08670 | Vimentin |
| *Chaperones (5)* | |
| P08238 | Heat shock protein HSP 90-β |
| P11142 | Heat shock cognate 71 kDa protein |
| P40227 | T-complex protein 1 subunit-æ |
| Q9UHV9 | Prefoldin subunit 2 |
| *Translation (2)* | |
| P60842 | Eukaryotic initiation factor 4A-I |
| P08865 | 40S ribosomal protein SA |
| Q13765 | Nascent polypeptide-associated complex subunit-α |
| *RNA binding proteins (1)* | |
| O00571 | ATP-dependent RNA helicase DDX3X |
| *Ub/Proteasome (1)* | |
| Q99460 | 26S proteasome non-ATPase regulatory subunit 1 |
| *Signaling (7)* | |
| P61981 | 14-3-3 protein γ |
| P52565 | Rho GDP-dissociation inhibitor 1 |
| P81605 | Dermcidin |
| Q92734 | Protein TFG |
| Q13795 | ADP-ribosylation factor-related protein 1 |
| P01024 | Complement C3 |
| P54756 | Ephrin type-A receptor 5 |
| *Trafficking (4)* | |
| P48444 | Coatomer subunit δ |
| P62820 | Ras-related protein Rab-1A |
| P20340 | Ras-related protein Rab-6A |
| Q9BY43 | Charged multivesicular body protein 4a |
| | |
| Organelles (9) | |
| *Endoplasmic reticulum (2)* | |
| P11021 | 78 kDa glucose-regulated protein |
| Q01105 | Protein SET |
| *Nucleus (6)* | |
| P45973 | Chromobox protein homolog 5 |
| P06748 | Nucleophosmin |
| P60174 | Triosephosphate isomerase |
| Q12905 | Interleukin enhancer-binding factor 2 |
| Q9UNZ2 | NSFL1 cofactor p47 |

## Table 1 Continued

| Accession no. | Identified protein[a] |
| --- | --- |
| Q99733 | Nucleosome assembly protein 1-like 4 |
| Q56NI9 | N-acetyltransferase ESCO2 |
| Q9BS16 | Centromere protein K |
| *Others (13)* | |
| P08758 | Annexin A5 |
| P02792 | Ferritin light chain |
| Q15181 | Inorganic pyrophosphatase |
| P09211 | Glutathione S-transferase P |
| O95394 | Phosphoacetylglucosamine mutase |
| O75223 | γ-Glutamylcyclotransferase |
| P07741 | Adenine phosphoribosyltransferase |
| P50452 | Serpin B8 |
| Q9NS25 | Sperm protein associated with the nucleus on the X chromosome B/F |
| Q9P1Z9 | Uncharacterized protein KIAA1529 (also known as TDRD7) |
| Q9H0J4 | Glutamine-rich protein 2 |
| Q9NQ48 | Leucine zipper transcription factor-like protein 1 |
| Q8IUR5 | Transmembrane and TPR repeat-containing protein 1 |

TDRD7, tudor domain containing 7.
The numeric character in the parentheses means the numbers of identified proteins for each group.
[a]Protein list, supportive information for protein identification, and functional classification are detailed in Supplementary Tables.

expression and knockdown experiments were conducted on MDA-MB-231 cells on the 3 μm porous membrane with the conditioned medium followed by western blotting. We subcloned the RAB1A cDNA into the mammalian expression vector, pCX4-bsr and the RAB1A-targetting siRNA into pSilencer4.1-CMVneo. Western blot analyses revealed that MDA-MB-231 cells overexpressed RAB1A when the cells were transfected with RAB1A cDNA plasmid, whereas RAB1A expression was faint with RAB1A-targetting siRNA (Supplementary Figure S5a). Moreover, the longer pseudopodial microprocesses with phalloidin staining were observed in the RAB1A-overexpressed cells and the fewer and shorter microprocesses were in the RAB1A-knockdown cells compared with the nontransfected cells using confocal microscopy (Supplementary Figure S5b and c).

## DISCUSSION

Identification of proteins associated with psuedopodia structure and functions will lead to a further understanding of cell migration. Tumor cell migration is involved in a critical part of invasion and metastasis. Therefore, such proteins for tumor cells can be considered as a candidate of molecular biomarkers and therapeutic targets. We demonstrated that the combined use of the medical laser technology
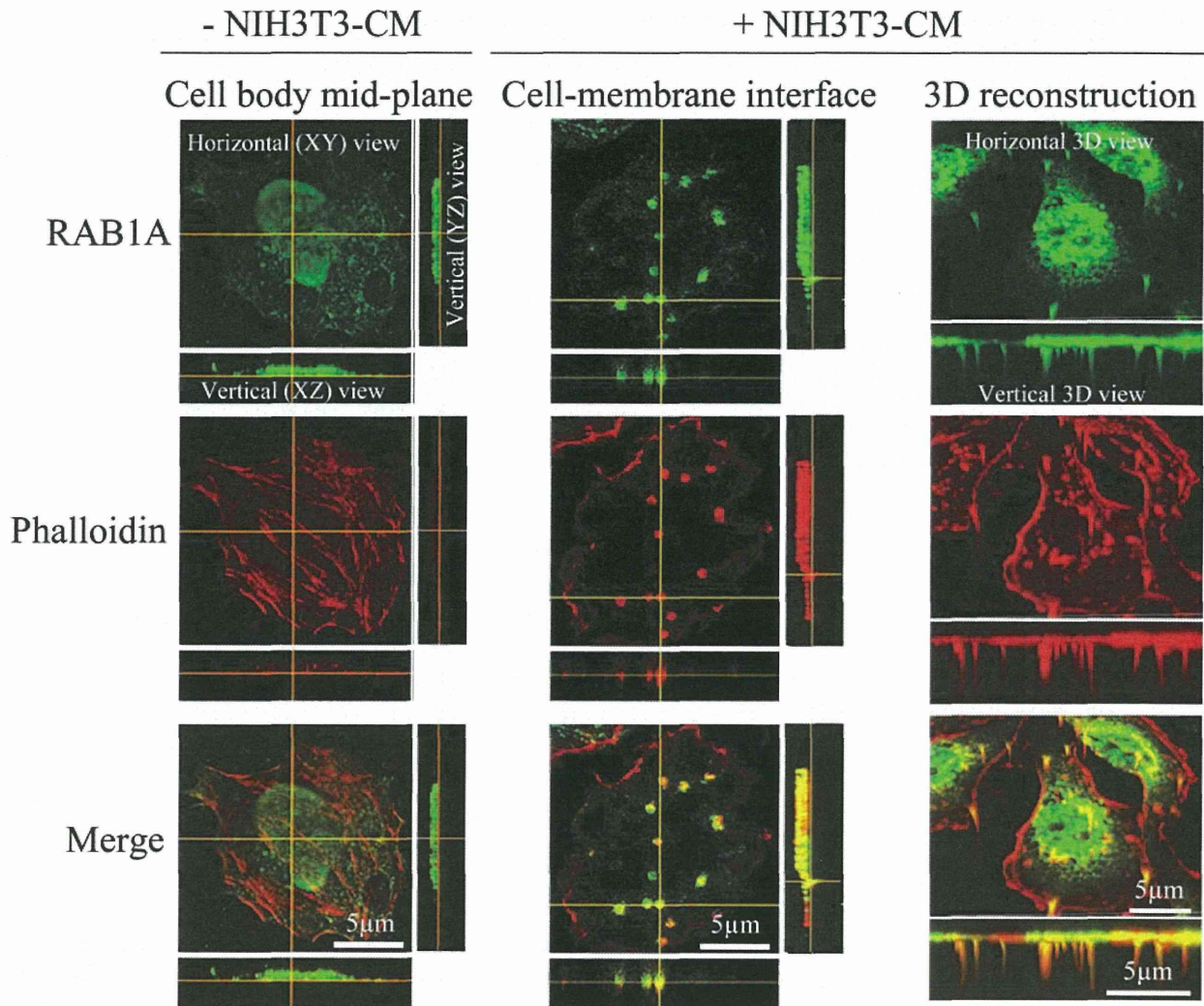
**Figure 3** Immunohistochemical view of RAB1A in pseudopodia. Localization of RAB1B before and after treatment with NIH3T3-conditioned medium was determined using immunohistochemical staining. Phalloidin staining was performed to visualize F-actin as a control in pseudopodial microprocesses. Note that RAB1A was observed as a dot-like structure in the horizontal view and as a protrusion in the vertical view following stimulation by NIH3T3-conditioned medium. RAB1A colocalized with F-actin after treatment and was detectable throughout the microprocess.

and the highly sensitive proteomics modalities identified a scarce amount of pseudopodia proteins.

When the cell body was removed by an excimer laser-assisted cell etching technique, there was no obvious damage on the pseudopodia appearances (Figure 1c) and the proteins in the pseudopodia remained intact (Figure 1d). This observation is supported by photochemistry and photophysics backgrounds. The laser keratectomy system used in this study was equipped with an argon fluoride excimer laser with a wavelength of 193 nm. Absorption at this wavelength is due primarily to peptide bonds ($O = CNN$) in the backbone of proteins in the cell rather than to water. Moreover, the optical absorption depth of the cell at 190 nm is estimated to be $\sim 500$ nm.[20] This suggests that protein degradation

can be induced only within a depth of 500 nm from the base of the pseudopodia. Additionally, pore size of the porous membrane (1 or 3 $\mu$m) is small relative to the excimer laser wavelength, that is, $\leq 15.5$ times as large as the wavelength (193 nm). This causes the membrane to exhibit a strong light-scattering effect at a wavelength of 193 nm. As a consequence, the excimer laser pulses cannot penetrate into the pores. With these backgrounds and experimental observations, we concluded that the excimer laser ablation did not cause significant protein degradation in the pseudopodia.

Using 2D-DIGE and high sensitive fluorescent dye, we can perform global protein expression studies. Indeed, only a few micrograms of proteins were enough to investigate the psuedopodia-associated proteins in this study. However,
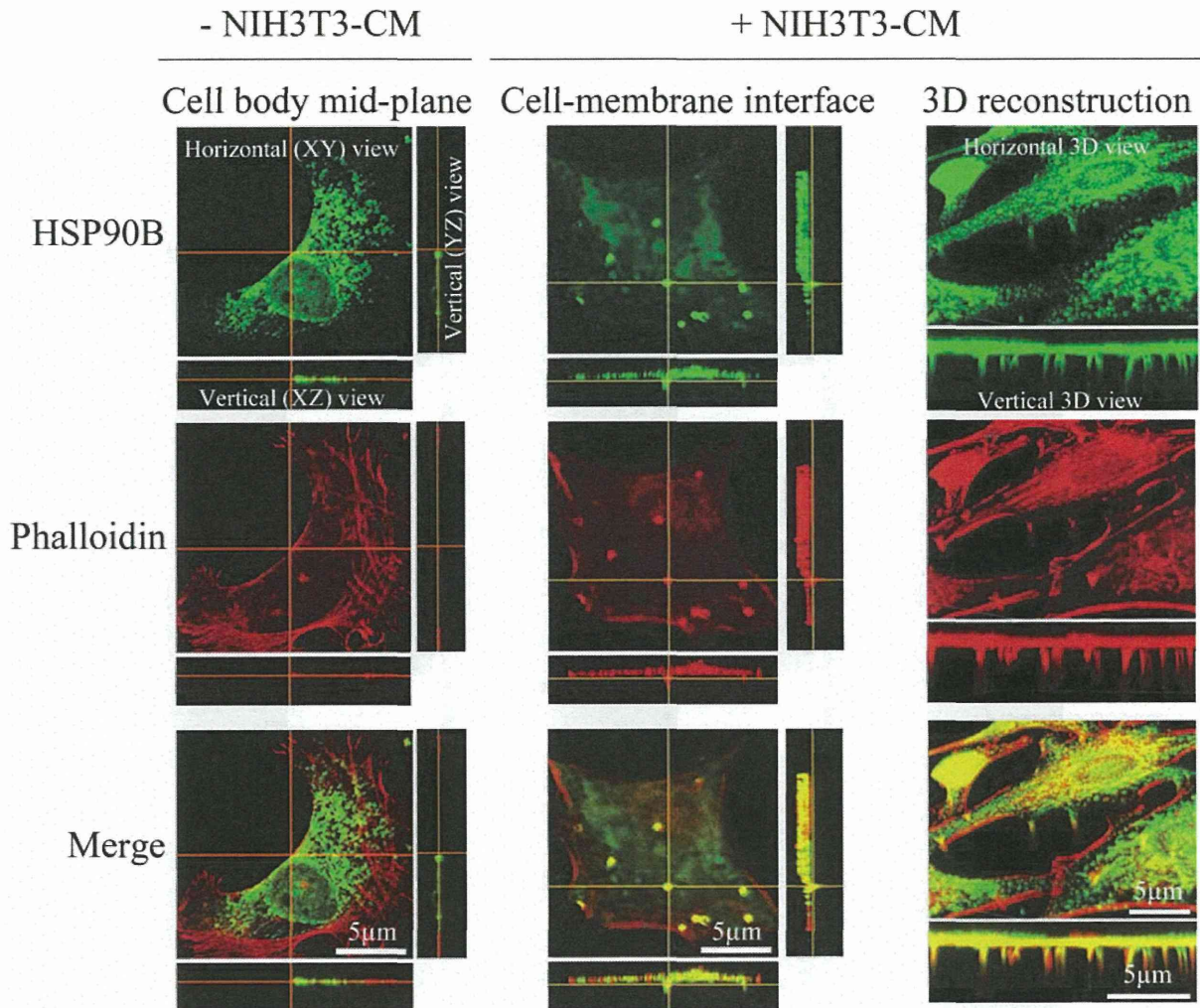
**Figure 4** Immunohistochemical view of HSP90B in pseudopodia. Localization of HSP90B without and with treatment with NIH3T3-conditioned medium was determined using immunohistochemical staining. Phalloidin staining was performed to visualize F-actin as a control protein in pseudopodial microprocesses. Note that HSP90B was observed as dot-like structures in the horizontal view and as protrusions in the vertical view after stimulation using NIH3T3-conditioned medium. HSP90B colocalized with F-actin after treatment and was detectable throughout the microprocess.

2D-DIGE allows observation of the proteins with middle to high expression level. This is because of the fact that 2D-DIGE does not select the proteins, and the proteins are detected in the order of expression level. In the case of mass spectrometry-based proteomics, several hundred micrograms of proteins are required for quantitative protein expression profiling, and psuedopodia proteins may not be investigated in a quantitative way. In addition, mass spectrometry also visualizes proteins in the order of expression level, and proteins with low expression may not be observed. Antibody-based proteomics such as antibody array can achieve sensitive and quantitative expression study. We may be able to observe proteins of small amount such as receptors and kinases. However, antibody-based proteomics generally requires much amount of proteins, and cannot be applied for the

study of pseudopodia proteins. Taken all together, we concluded that 2D-DIGE is a best method among the proteomics modalities for psuedopodia proteomics.

Among identified proteins, 12 highly expressed proteins in PME molecules, including cytoskeletal and chaperone proteins, were also identified in a past report involving pseudopodial proteomics.[4] This finding indicated that the present new method certainly examined pseudopodia. On the other hand, pseudopodia in the 1 μm pore may morphologically seem to be a part of that in the 3 μm pore. This speculation was supported by the observation that most identified molecules in PME-1 were observed in PME-3. The overlapped proteins may be most specific candidate molecules that lead or promote cell migration. On the other hand, several identified proteins, such as TDRD7 and
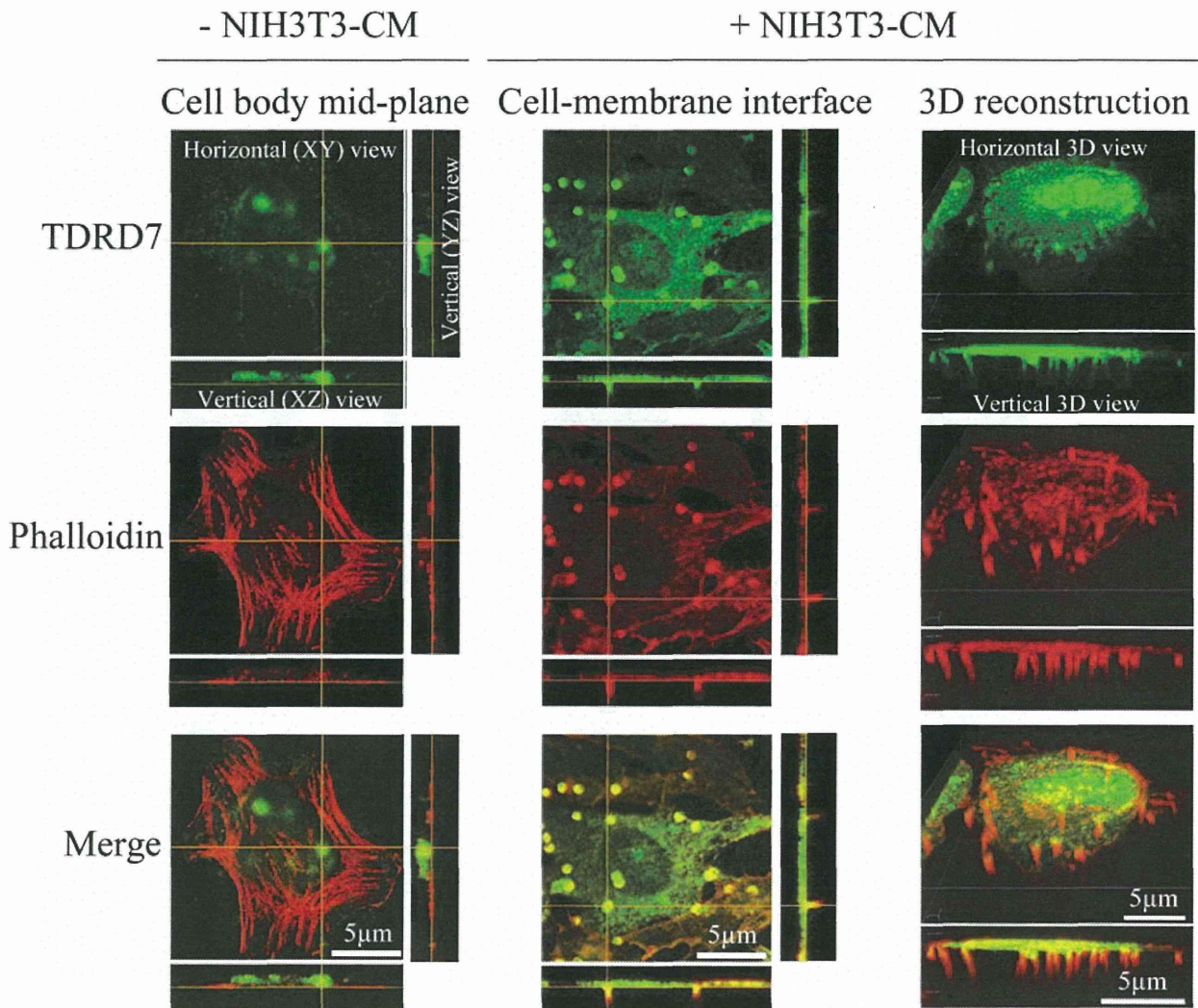
**Figure 5** Immunohistochemical view of TDRD7 in pseudopodia. Localization of TDRD7 without and with treatment using NIH3T3-conditioned medium was determined using immunohistochemical staining. Phalloidin staining was performed to visualize F-actin as a control protein in pseudopodial microprocesses. Note that TDRD7 was observed as dot-like structures in the horizontal view and as protrusions in the vertical view after stimulation using NIH3T3-conditioned medium. TDRD7 colocalized with F-actin after treatment and was primarily located in the proximal region of the microprocess.

vimentin, were identified in both 'upregulated proteins' and 'downregulated proteins' in PME compared with WCE. One considerable reason is that specific forms of TDRD7 and vimentin are differently regulated between pseudopodia and cell body. The variations of protein spots may reflect the different posttranslational modifications, and they may play distinct roles in cell behaviors. Further characterization of their posttranslational modifications in relation to psuedopodia should be an interesting subject, although it is not easy because of the sensitivity of mass spectrometry and a lack of methods to control the expression of specific protein forms.

In the present study, the localization of RAB1A, HSP90B, TDRD7, and vimentin in the pseudopodia with actin stress fiber, which is known to be enriched in pseudopodia,[1,2]

was confirmed by immunohistochemical experiment (Figures 3–6). In addition, RAB1A was indicated to play an important role in forming and extending pseudopodial microprocesses in human breast cancer cells by overexpression and knockdown experiments. Previous studies demonstrated that these four proteins may function in the process of cell migration. HSP90B is known to function as a chaperone for proper folding of integrin molecules.[21,22] Vimentin filaments are shown to be connected to integrin matrix adhesion sites.[23] Interestingly, guanosine triphosphatase activity of RAB1A and N-terminal phosphorylation of vimentin filaments are involved in vesicle trafficking of integrins to the plasma membrane.[24] Although the specific function is still unknown, TDRD7 is a scaffold for various proteins including
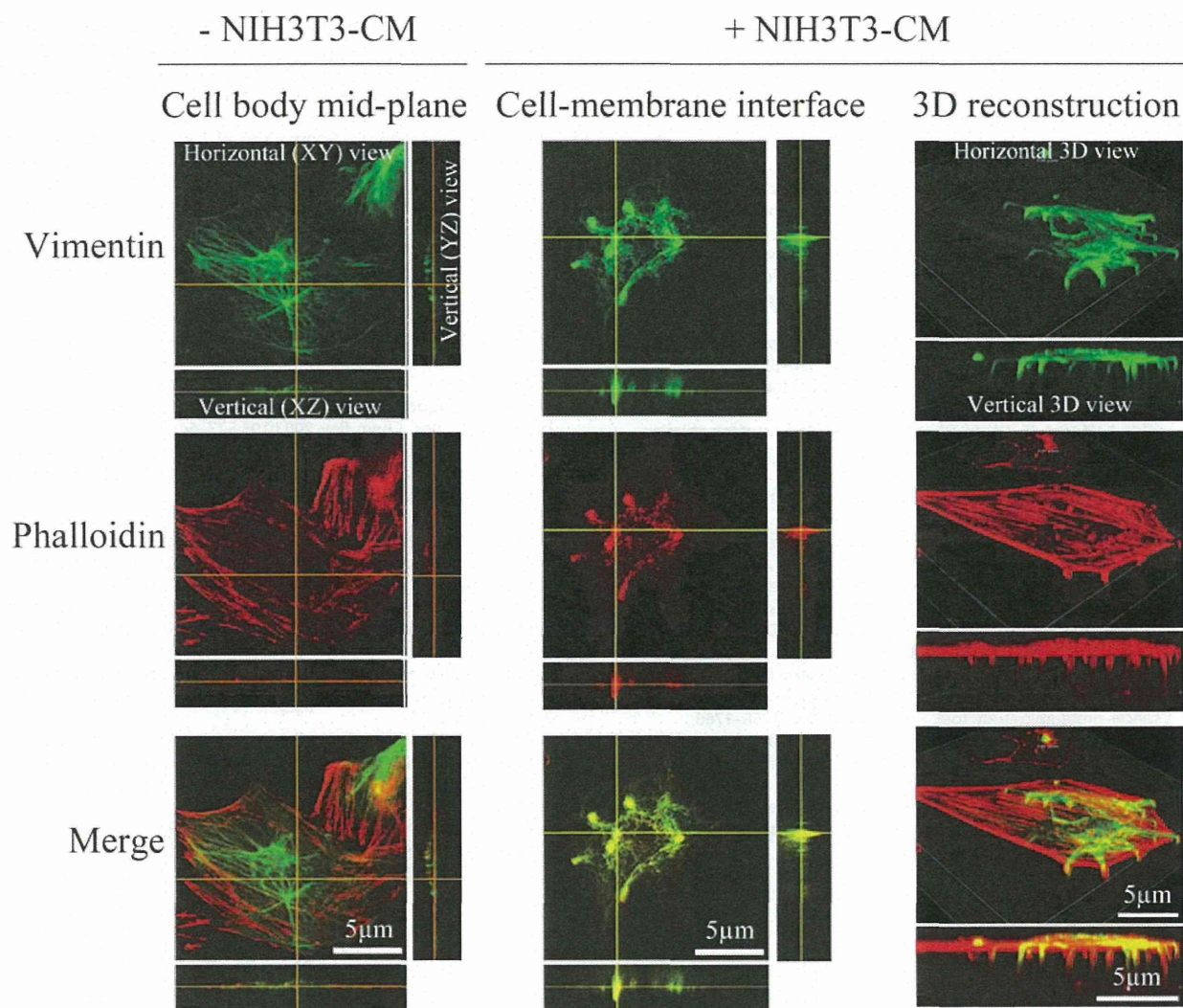
**Figure 6** Immunohistochemical view of vimentin in pseudopodia. Localization of vimentin without and with treatment using NIH3T3-conditioned medium was determined using immunohistochemical staining. Phalloidin staining was performed to visualize F-actin as a control protein in pseudopodial microprocesses. Note that vimentin was observed as dot-like structures in the horizontal view and as protrusions in the vertical view after stimulation using NIH3T3-conditioned medium. Vimentin colocalized with F-actin after treatment and was primarily located in the proximal region of the microprocess.

Ser/Thr kinase PCTAIRE 2[25] and TACC1.[26] Thus, these four proteins may participate in integrin-dependent pseudopodia formation and directional cell migration. Their functional role for pseudopodia and possible clinical utilities are worth investigating in further studies.

In conclusion, we established a novel application for pseudopodia proteomics by using a fully developed medical nanodevice and a proteomic modality. Proteomics showed pseudopodia to be dynamic cellular components involved in cytoskeletal remodeling, protein synthesis, trafficking, and degradation as well as involved in various signal transduction pathways. We observed significant proteomic differences between pseudopodia of different diameters and between cell lines with different motile potentials. We confirmed novel pseudopodial localization of RAB1A, HSP90B, TDRD7, and vimentin, which play an important role in cell migration. Additional proteomic studies using varying pore sizes of membranes and different cell types, followed by functional studies of the identified proteins, will reveal the precise molecular basis of cell migration.

Supplementary Information accompanies the paper on the Laboratory Investigation website (http://www.laboratoryinvestigation.org)

## DISCLOSURE/CONFLICT OF INTEREST

The authors declare no conflict of interest.

1. Lauffenburger DA, Horwitz AF. Cell migration: a physically integrated molecular process. Cell 1996;84:359–369.
2. Parent CA, Devreotes PN. A cell's sense of direction. Science 1999;284: 765–770.
3. Nguyen TN, Wang HJ, Zalzal S, *et al*. Purification and characterization of beta-actin-rich tumor cell pseudopodia: role of glycolysis. Exp Cell Res 2000;258:171–183.
4. Jia Z, Barbier L, Stuart H, *et al*. Tumor cell pseudopodial protrusions. Localized signaling domains coordinating cytoskeleton remodeling, cell adhesion, glycolysis, RNA translocation, and protein translation. J Biol Chem 2005;280:30564–30573.
5. Wang Y, Ding SJ, Wang W, *et al*. Profiling signaling polarity in chemotactic cells. Proc Natl Acad Sci USA 2007;104:8328–8333.
6. Wang Y, Ding SJ, Wang W, *et al*. Methods for pseudopodia purification and proteomic analysis. Sci STKE 2007;2007:pl4.
7. Reynolds A, Moore JE, Naroo SA, *et al*. Excimer laser surface ablation - a review. Clin Experiment Ophthalmol 2010;38:168–182.
8. Solomon KD, Fernandez de Castro LE, Sandoval HP, *et al*. LASIK world literature review: quality of life and patient satisfaction. Ophthalmology 2009;116:691–701.
9. Hanash S, Taguchi A. The grand challenge to decipher the cancer proteome. Nat Rev Cancer 2010;10:652–660.
10. Kondo T, Hirohashi S. Application of highly sensitive fluorescent dyes (CyDye DIGE Fluor saturation dyes) to laser microdissection and two-dimensional difference gel electrophoresis (2D-DIGE) for cancer proteomics. Nat Protoc 2007;1:2940–2956.
11. Kondo T, Seike M, Mori Y, *et al*. Application of sensitive fluorescent dyes in linkage of laser microdissection and two-dimensional gel electrophoresis as a cancer proteomic study tool. Proteomics 2003;3:1758–1766.
12. Shaw J, Rowlinson R, Nickson J, *et al*. Evaluation of saturation labelling two-dimensional difference gel electrophoresis fluorescent dyes. Proteomics 2003;3:1181–1195.
13. Unlu M, Morgan ME, Minden JS. Difference gel electrophoresis: a single gel method for detecting changes in protein extracts. Electrophoresis 1997;18:2071–2077.
14. Kondo T, Hirohashi S. Application of 2D-DIGE in cancer proteomics toward personalized medicine. Methods Mol Biol 2009;577:135–154.
15. Ito A, Kataoka TR, Watanabe M, *et al*. A truncated isoform of the PP2A B56 subunit promotes cell motility through paxillin phosphorylation. EMBO J 2000;19:562–571.
16. Du CX, Shen Y, Wang Y. Comparison of high order aberration after conventional and customized ablation in myopic LASIK in different eyes of the same patient. J Zhejiang Univ Sci B 2007;8:177–180.
17. Victor G, Urbano A, Marcal S, *et al*. [First Brazilian refractive surgery survey]. Arq Bras Oftalmol 2005;68:727–733.
18. Akagi T, Murata K, Shishido T, *et al*. v-Crk activates the phospho-inositide 3-kinase/AKT pathway by utilizing focal adhesion kinase and H-Ras. Mol Cell Biol 2002;22:7015–7023.
19. Kong T, Xu D, Yu W, *et al*. G alpha 12 inhibits alpha2 beta1 integrin-mediated Madin-Darby canine kidney cell attachment and migration on collagen-I and blocks tubulogenesis. Mol Biol Cell 2009;20: 4596–4610.
20. Vogel A, Venugopalan V. Mechanisms of pulsed laser ablation of biological tissues. Chem Rev 2003;103:577–644.
21. Liu B, Li Z. Endoplasmic reticulum HSP90b1 (gp96, grp94) optimizes B-cell function via chaperoning integrin and TLR but not immunoglobulin. Blood 2008;112:1223–1230.
22. Morales C, Wu S, Yang Y, *et al*. Drosophila glycoprotein 93 is an ortholog of mammalian heat shock protein gp96 (grp94, HSP90b1, HSPC4) and retains disulfide bond-independent chaperone function for TLRs and integrins. J Immunol 2009;183:5121–5128.
23. Gonzales M, Weksler B, Tsuruta D, *et al*. Structure and function of a vimentin-associated matrix adhesion in endothelial cells. Mol Biol Cell 2001;12:85–100.
24. Ivaska J, Pallari HM, Nevo J, *et al*. Novel functions of vimentin in cell adhesion, migration, and signaling. Exp Cell Res 2007;313: 2050–2062.
25. Hirose T, Kawabuchi M, Tamaru T, *et al*. Identification of tudor repeat associator with PCTAIRE 2 (Trap). A novel protein that interacts with the N-terminal domain of PCTAIRE 2 in rat brain. Eur J Biochem 2000;267:2113–2121.
26. Conte N, Delaval B, Ginestier C, *et al*. TACC1-chTOG-Aurora A protein complex in breast cancer. Oncogene 2003;22:8102–8116.

**JSHC**
Japan Society of
Histochemistry and Cytochemistry
Established 1959

# Compensatory Upregulation of Myelin Protein Zero-Like 2 Expression in Spermatogenic Cells in Cell Adhesion Molecule-1-Deficient Mice

**Hiroki Nakata[1], Tomohiko Wakayama[1], Kannika Adthapanyawanich[1], Takumi Nishiuchi[2], Yoshinori Murakami[3], Yoshimi Takai[4] and Shoichi Iseki[1]**

[1]Department of Histology and Embryology, Graduate School of Medical Science, Kanazawa University, 13–1 Takara-machi, Kanazawa, Ishikawa 920–8640, Japan, [2]Division of Functional Genomics, Advanced Science Research Center, Kanazawa University, 13–1 Takaramachi, Kanazawa, Ishikawa 920–8640, Japan, [3]Division of Molecular Pathology, Department of Cancer Biology, Institute of Medical Science, The University of Tokyo, 4–6–1, Shirokanedai, Minato-ku, Tokyo 108–8639, Japan and [4]The Division of Molecular and Cellular Biology, Department of Biochemistry and Molecular Biology, Kobe University Graduate School of Medicine, Kobe, Hyogo 650–0017, Japan

The cell adhesion molecule-1 (Cadm1) is a member of the immunoglobulin superfamily. In the mouse testis, Cadm1 is expressed in the earlier spermatogenic cells up to early pachytene spermatocytes and also in elongated spermatids, but not in Sertoli cells. Cadm1-deficient mice have male infertility due to defective spermatogenesis, in which detachment of spermatids is prominent while spermatocytes appear intact. To elucidate the molecular mechanisms of the impaired spermatogenesis caused by Cadm1 deficiency, we performed DNA microarray analysis of global gene expression in the testis compared between Cadm1-deficient and wild-type mice. Out of the 25 genes upregulated in Cadm1-deficient mice, we took a special interest in myelin protein zero-like 2 (Mpzl2), another cell adhesion molecule of the immunoglobulin superfamily. The levels of Mpzl2 mRNA increased by 20-fold and those of Mpzl2 protein increased by 2-fold in the testis of Cadm1-deficient mice, as analyzed with quantitative PCR and western blotting, respectively. *In situ* hybridization and immuno-histochemistry demonstrated that Mpzl2 mRNA and protein are localized in the earlier spermatogenic cells but not in elongated spermatids or Sertoli cells, in both wild-type and Cadm1-deficient mice. These results suggested that Mpzl2 can compensate for the deficiency of Cadm1 in the earlier spermatogenic cells.

**Key words:** cell adhesion molecule, immunoglobulin superfamily, knockout mouse, spermatogenesis, testis

## I.  Introduction

Spermatogenesis is a complex process consisting of mitosis of spermatogonia, meiosis of spermatocytes, and transformation of spermatids (spermiogenesis) which occurs within the seminiferous tubule. It is well established that spermatogenesis is regulated by a variety of endocrine and local secretory factors [13]. Another essential factor for the regulation of spermatogenesis is cell adhesion molecules responsible for the direct interaction between spermatogenic and Sertoli cells. Apical ectoplasmic specialization (ES) is a structure formed between elongated spermatids and Sertoli cells near the apical surface of seminiferous epithelium. Several cell adhesion molecules are known to be involved in the apical ES [15, 16, 27]. Most of these molecules belong to the immunoglobulin superfamily (IGSF), which is characterized by extracellular regions that contain immunoglobulin (Ig)-like domains [2]. Studies using knockout mice have indicated that deficiency of some of

Correspondence to: Shoichi Iseki, Department of Histology and Embryology, Graduate School of Medical Science, 13–1 Takara-machi, Kanazawa 920–8640, Japan.
E-mail: siseki@med.kanazawa-u.ac.jp

the IGSF molecules, such as junctional adhesion molecule-C (Jam-C), Nectin-2 and Nectin-3, leads to male infertility due to impaired spermatogenesis [6, 8, 14].

Cell adhesion molecule-1 (Cadm1), originally reported as spermatogenic immunoglobulin superfamily (SgIGSF) [22], tumor suppressor in lung cancer 1 (Tslc1) [10] and nectin-like molecule-2 (Necl-2) [18], is a member of the IGSF and expressed in many mouse organs including the nervous system, testis, liver, and lung [24]. In the testis, Cadm1 is expressed exclusively in spermatogenic cells but not in Sertoli cells. In spermatogenic cells, Cadm1 is expressed in intermediate spermatogonia through to early pachytene spermatocytes as well as in step 7 and later spermatids, whereas it is not expressed in middle pachytene through to step 6 spermatids [23, 24, 26]. Cadm1 not only forms homophilic binding with the same molecule present on spermatogenic cells, but also heterophilic binding with another cell adhesion molecule poliovirus receptor (Pvr), that is present on Sertoli cells [23, 26]. Mice deficient for Cadm1 are infertile due to impaired spermatogenesis with markedly reduced number of mature spermatozoa [5, 20, 21, 28], indicating that the cell-cell interaction involving Cadm1 plays an indispensable role in spermatogenesis. Histologically, the seminiferous epithelium of Cadm1-deficient mice indicates prominent shedding of spermatids, particularly of step 7 to step 9 spermatids, into the lumen of seminiferous tubules [5, 21, 27, 28]. Also, the elongated spermatids remaining in the seminiferous tubules are irregular in shape and have incompletely condensed nuclei and poorly-developed flagella, indicating abnormal spermatid differentiation. In contrast, the earlier spermatogenic cells from intermediate spermatogonia through to early pachytene spermatocytes, despite the fact that these cells express Cadm1 in wild-type mice, appear to be intact. Such a phenotype of Cadm1-deficient mice may not be explained simply by the loss of cell-cell contact due to Cadm1 deficiency.

In the present study, we aimed to elucidate the molecular mechanisms underlying the impaired spermatogenesis in Cadm1-deficient mice. For this purpose, we investigated the global gene expression in the testis from Cadm1-deficient mice compared with that from wild-type mice, using the DNA microarray technique. We identified upregulation of the gene for myelin protein zero-like 2 (Mpzl2), another IGSF cell adhesion molecule, in the testis of Cadm1-deficient mice, and analyzed the expression and localization of Mpzl2 in the seminiferous tubules.

## II.  Materials and Methods

### Animals and tissue preparation

All animal experiments were performed according to Guidelines for the Care and Use of Laboratory Animals in Kanazawa University. Cadm1-deficient 129Sv/C57BL6 strain mice (Cadm1–/–), which lack the entire exon 1 of the Cadm1 gene located on #9 autonomic chromosome, were generated as described previously [26]. Male Cadm1-

deficient mice were obtained by mating the female Cadm1+/– with the male Cadm1+/–, and male wild-type mice (Cadm1+/+) were also reared for use as control. Nectin-3-deficient 129Sv/C57BL6 strain mice were generated as described previously [8]. In total, 22 Cadm1-deficient, 22 wild-type, and 3 Nectin-3-deficient male mice were used to obtain the present data. Unless otherwise indicated, the adult mice were used at the ages of 15 to 20 wk. Two female WKY/NCrj Wistar rats at 10 wk were purchased from Charles River Laboratories Japan, Inc. (Yokohama, Japan) for immunization. All animals were raised under standard laboratory conditions with a 12 hr-light/12 hr-dark cycle and free access to food and water. The mice were anesthetized with an intraperitoneal injection of sodium pentobarbital (50 mg/kg) and sacrificed by bleeding from the right atrium followed by transcardial perfusion with cold physiological saline. To isolate total RNA for microarray and reverse transcription-polymerase chain reaction (RT-PCR) or to make cell lysates for Western blotting, the testes were dissected out, frozen immediately in liquid nitrogen, and stored at –80°C until use. To make tissue sections, the animals were fixed by perfusion with cold 4% paraformaldehyde in 0.1 M phosphate buffer (pH 7.2), testes were dissected out and further fixed by immersion in the same fixative overnight at 4°C. For in situ hybridization (ISH) and immunohistochemistry (IHC), the fixed specimens were rinsed overnight at 4°C with 30% sucrose in 0.1 M phosphate buffer and then frozen and cut into 8 μm sections using a cryostat. Some fixed specimens were embedded in paraffin and cut into 4 μm sections for PAS-hematoxylin staining. The sections were mounted on silanized glass slides (DAKO, Glostrup, Denmark).

### RNA preparation and microarray analysis

Total RNA was isolated from the testis using an acid guanidinium-based solution (TRI reagent; Sigma-Aldrich, St. Louis, MO). For the microarray analysis, total RNA of testes from 3 animals in each experimental condition were mixed to represent each total RNA sample. Microarray experiment was performed using Whole Mouse Genome oligo DNA microarray kit (Agilent Technologies, Santa Clara, CA, USA) containing 44,000 probes for mouse genes according to the manufacturer's protocol. One μg-aliquots of total RNA samples from the testes of wild-type and Cadm1-deficient mice were used to prepare Cy3- and Cy5-labeled cRNAs, respectively, using a fluorescent labeling kit (Agilent Technologies). The two sets of fluorescent labeled cRNAs were combined and purified using an RNeasy RNA purification kit (Qiagen, Hilden, Germany). After hybridization with the cRNA solution and washing, the arrays were scanned under the maximum laser intensity for both the Cy3 and Cy5 channels using an Agilent microarray scanner (G2565BA). Images were analyzed using Feature Extraction software (version 7.0; Agilent Technologies).

### RT-PCR and quantitative RT-PCR

First-strand cDNA was synthesized from a 1 μg-aliquot

of the total RNA from each animal using the oligo-dT primer and reverse transcriptase (RT) (RevertraAce; Toyobo, Osaka, Japan). Using these cDNA samples, the conventional RT-PCR was performed for 28 cycles in a DNA thermal cycler (96-Well GeneAmp PCR System 9700; Applied Biosystems, Foster City, CA, USA), using Taq DNA polymerase (TaKaRa Ex Taq; Takara Bio Inc., Otsu, Shiga) and the following primer pairs: the Mpzl2 5'-primer (5'-CT ATGCAGTGTTGGCCTGAA-3'), the Mpzl2 3'-primer (5'-TGTTGAGCTGGGGGTAAAAG-3'), the glyceraldehyde-3-phosphate dehydrogenase (GAPDH) 5'-primer (5'-ACCA CAGTCCATGCCATCAC-3'), and the GAPDH 3'-primer (5'-TCCACCACCCTGTTGCTGTA-3'). The amplified products from 3 different animals were analyzed with agarose-gel electrophoresis.

Quantitative RT-PCR was performed in a Stratagene Mx-3005P thermocycler (Stratagene, La Jolla, CA, USA) according to minimum information for publication of quantitative real-time PCR experiments (MIQE). SYBR green was used to detect the amplification of cDNA in a total volume of 20 μl with the absolute quantitative, ΔCt method [17]. Each reaction consisted of 10 μl of SYBR green, 1 μl of cDNA sample, 0.5 μl of each primer pair (10 pmol/μl), and 8 μl of distilled water. Thermal cycling conditions were 10 min at 95°C followed by 45 cycles at 95°C for 40 sec, 60°C for 30 sec, and 72°C for 30 sec. GAPDH was employed as an endogenous control to normalize the data. Each sample was analyzed in triplicates, and samples from 3 different animals were analyzed to determine each value.

*In situ hybridization (ISH)*

An oligonucleotide containing digoxigenin (DIG)-labeled locked nucleic acid (LNA) (5'-AggGgggggggaGg gagagaAataaA-3'; large capitals represent LNA) was purchased from Nippon EGT (Toyama) and used as the antisense probe for Mpzl2 mRNA. Melting temperature (Tm) of this LNA probe was predicted to be 75°C using the LNA Tm prediction tool which is accessible at http://lna-tm.com. The antisense and sense LNA probes without DIG label were also used. ISH was performed as previously described [22]. Briefly, the 4% paraformaldehyde-fixed cryostat sections of the mouse testis were treated successively at room temperature with proteinase K (10 μg/ml) in Tris-EDTA buffer for 2 min, and with 0.25% acetate anhydrate in 0.1 M triethanolamine (pH 8.0) for 10 min, washed in 4×sodium chloride/sodium citrate (SSC) and dehydrated in ethanol. The sections were then incubated with the DIG-labeled antisense probe (10 pmol/L) at 37°C for 15 hr using a hybridization buffer containing 50% deionized formamide, 2×SSC, 10 mM Tris-HCl (pH 7.5), 1 mM EDTA (pH 8.0), 1×Denhardt's solution, 0.25% SDS, 250 μg/ml yeast tRNA and 10% dextran sulfate. As control, the excess of unlabelled antisense or sense probe (1000 pmol/L) were added to DIG-labeled antisense probe. After hybridization, the tissue sections were washed in 0.2×SSC containing 2% bovine serum albumin at 37°C for 5 min.

The hybridization signals were detected by incubating the sections successively with alkaline phosphatase-conjugated anti-DIG antibody (Roche Diagnostics, Basel, Switzerland) diluted at 1:600 in 0.1 M Tris-HCl, 150 mM NaCl, pH 7.5 and with the substrate Fast Red (DAKO, Glostrup, Denmark) in 50 mM Tris-HCl (pH 9.5). The ISH results were confirmed in the testes from 3 different animals. To identify the stages of seminiferous tubules, some sections were stained in the acrosome with Alexa Fluor 488-conjugated lectin PNA (1:500; Molecular Probes, Eugene, OR, USA) and counter-stained in the nucleus with bisbenzimide (Hoechst 33258; Sigma-Aldrich) at 100 ng/ml.

*Preparation of primary antibodies*

Rabbit polyclonal anti-Cadm1 antibody was prepared as previously described [23]. Mouse monoclonal anti-α-tubulin (clone DM 1A) antibody was purchased from Sigma-Aldrich. Rat polyclonal antisera against mouse Mpzl2 was produced in our laboratory according to the method described previously, with modification [25]. Briefly, a cDNA fragment 96 bp in length coding the carboxyl-termini of mouse Mpzl2 was cloned into the bacterial expression vector pGEX-6p-1 (Amersham Pharmacia Biotech, Uppsala, Sweden). By introducing this vector into the bacteria BL21 (Novagen, Madison, WI, USA), the recombinant oligo-peptide for Mpzl2, which was 32-amino acids in length and fused with the carrier protein glutathione-S-transferase (GST), was produced. It was then emulsified with Freund's complete adjuvant and injected as antigen into the footpads of 2 female WKY/NCrj Wistar rats. A booster immunization was made two weeks later, and sera were collected one week after the booster.

*Western-blot analysis*

Western blotting was performed as previously described [27]. Twenty-μg aliquots of cell lysate from the mouse testis were subjected to SDS-PAGE and transferred to PVDF membranes (Bio-Rad Laboratories, Hercules, CA, USA). The blots were incubated with rat polyclonal antisera against mouse Mpzl2 (1:2000) or mouse monoclonal anti-α-tubulin antibody (1:2000). After being washed, the blots were further incubated with horseradish peroxidase-labeled secondary antibody against rat or mouse IgG (DAKO) at 1:5000 dilution. The immunoreaction was detected and its intensity was quantified in ImageQuant LAS-4000 mini (Fujifilm Medical, Tokyo) after treatment of the blots with the chemiluminescent reagent ECL-plus (Amersham Pharmacia Biotech). Samples from 3 different animals were analyzed to determine each value.

*Immunohistochemistry (IHC)*

IHC at the light microscopic level was performed as previously described [26]. Briefly, the 4% paraformal-dehyde-fixed cryostat sections of the mouse testis were first treated with 5% normal goat serum to prevent non-specific antibody binding and then incubated overnight at 4°C with rat polyclonal antisera against mouse Mpzl2 (1:800) for

single immunofluorescent microscopy, or with the mixture of the former antisera and rabbit polyclonal anti-Cadm1 antibody (10 µg/ml) for double immunofluorescent microscopy. For negative control, normal rat sera (1:800) were used in place of the primary antibodies. After the sections were washed in PBS, the immunoreaction was visualized by incubating the sections with anti-rat IgG antibody conjugated with Alexa Fluor 594 (Molecular Probes) at 1:400 for single immunofluorescent microscopy, or with the mixture of the former antibody and anti-rabbit IgG antibody conjugated with Alexa Fluor 488 at 1:400 for double immunofluorescent microscopy, for 1 hr at room temperature. The sections were then subjected to observation with an immunofluorescence microscope (BX50/BX-FLA; Olympus, Tokyo). The IHC results were confirmed in the testes from 3 different animals. To reveal the histological features of seminiferous tubules, the paraffin sections were stained with PAS-hematoxylin and subjected to observation with a conventional microscope.

### Statistical analysis

The statistical difference between two out of multiple mean values was examined by one-factor analysis of variance (ANOVA) followed by Bonferroni's post hoc test. Differences with a P value less than 0.05 were considered significant.

## III. Results

### Increased expression of Mpzl2 mRNA in the testis of Cadm1-deficient mice

To elucidate the molecular mechanisms underlying the impaired spermatogenesis caused by Cadm1 deficiency, we performed DNA microarray analysis of the levels of global gene expression in the testes from Cadm1-deficient mice at 2, 5 and 20 wk postpartum compared with those from wild-type counterparts. The rationale for adopting these ages was that, during the normal testis development, pachytene

spermatocytes with round shape and large nuclei first appear at 2 wk postpartum, and elongated spermatids (step 7 and later spermatids) at 5 wk postpartum, in the luminal portions of seminiferous epithelia [1]. The expressions of 25 and 21 genes were found to be increased and decreased more than 1.5-fold, respectively, at all three ages of Cadm1-deficient mice (Fig. 1A, B; Table 1). As expected, Cadm1 itself was included in the 21 down-regulated genes.

Taking into account that the testis of Cadm1-deficient mice is lacking in normal later spermatids, we considered the upregulated genes to be more worthwhile to investigate than the downregulated ones. Therefore, quantitative RT-PCR analysis was performed in the testes from adult wild-type and Cadm1-deficient mice on the mRNA for the 25 genes shown to be upregulated by DNA microarray analysis. The testis of Nectin-3-deficient mice, which are infertile due to impaired spermatogenesis, was also analyzed. We confirmed approximately 20-fold increase of the mRNA for Mpzl2 in the testis from adult Cadm1-deficient mice compared with wild-type mice (Fig. 2A, B). No significant difference was noted in the levels of Mpzl2 mRNA between wild-type and Nectin-3-deficient mice. The mRNA for Kcnd2, a potassium channel gene, was also confirmed to be increased by RT-PCR, but the mRNA for all other genes were expressed at too small copy numbers in the testis (data not shown).

### Localization of Mpzl2 mRNA in the testes of wild-type and Cadm1-deficient mice

We then examined the expression and cellular localization of Mpzl2 mRNA in the testes from wild-type and Cadm1-deficient adult mice with ISH analysis. We used a digoxigenin-labeled oligonucleotide probe containing LNA, a modified DNA nucleotide. LNA probes are known to increase the melting temperature and therefore the intensity and specificity of molecular hybridization. In the seminiferous tubules of wild-type mice, the signal for Mpzl2 mRNA was detected primarily in spermatocytes but not in sperma-
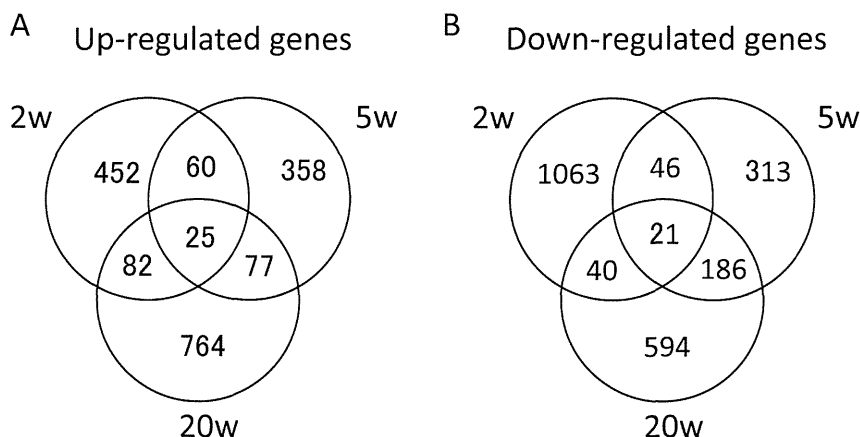


**Fig. 1.** Microarray analysis of the global gene expression in the testes of Cadm1-deficient mice at 2, 5 and 20 postnatal weeks (w) compared with those of wild-type mice.

**Table 1.** *List of up- and down-regulated genes in the testis common to all three ages of Cadm1-deficient mice compared with those of wild-type mice*

| Gene | NCBI accession no. | fold change |
|---|---|---|
| Kcnd2 | NM_019697 | 4.59 |
| Mpzl2 | NM_007962 | 4.55 |
| | | 2.13 |
| Gpr182 | NM_007412 | 2.02 |
| Blvrb | NM_144923 | 1.97 |
| Tnfaip6 | NM_009398 | 1.88 |
| Trim56 | NM_201373 | 1.85 |
| Ei24 | NM_007915 | 1.84 |
| Mdk | NM_010784 | 1.82 |
| Hspa8 | NM_031165 | 1.76 |
| Rnd2 | NM_009708 | 1.76 |
| Col18a1 | NM_009929 | 1.75 |
| Stt3a | NM_008408 | 1.63 |
| Trfr2 | NM_015799 | 1.63 |
| Atp1a2 | NM_178405 | 1.62 |
| Scrn2 | NM_146027 | 1.61 |
| Smoc2 | NM_022315 | 1.60 |
| Arhgef1 | NM_008488 | 1.57 |
| Tnfrsf12a | NM_013749 | 1.56 |
| Pla2g15 | NM_133792 | 1.56 |
| | AK010169 | 1.55 |
| Tuba3a | NM_009446 | 1.55 |
| Myoz2 | NM_021503 | 1.52 |
| 5730437N04Rik | NM_027457 | 1.51 |
| | AK085343 | 1.50 |
| Prkar2a | NM_008924 | 0.65 |
| | AK087842 | 0.65 |
| | AK006816 | 0.63 |
| | AK077682 | 0.63 |
| Clec4g | NM_029465 | 0.62 |
| | AK045399 | 0.62 |
| Odf2 | NM_013615 | 0.60 |
| Rplp1 | NM_018853 | 0.57 |
| Ptgds | NM_008963 | 0.56 |
| | BE990773 | 0.50 |
| Tctex2 | U21674 | 0.46 |
| Fez1 | NM_183171 | 0.44 |
| 9030425E11Rik | NM_133733 | 0.40 |
| Myom2 | NM_008664 | 0.36 |
| Pcsk7 | NM_008794 | 0.35 |
| | AK007186 | 0.34 |
| Hrasls5 | NM_025731 | 0.23 |
| Hddc3 | NM_026812 | 0.16 |
| Cadm1 | NM_207675 | 0.06 |
| Cadm1 | NM_207676 | 0.04 |
| Nicn1 gene | AJ299741 | 0.03 |

tids at all stages of the spermatogenesis defined by PNA lectin histochemistry (Fig. 3A, B). The signal intensity appeared to be increased in the seminiferous tubules of Cadm1-deficient mice compared with those of wild-type mice (Fig. 3C). No signal was detected in Sertoli cells,

judging from the absence of signal in the basal- and apical-most portions of seminiferous epithelium. The signal disappeared when excess unlabeled antisense or sense probe was added to the probe solution for negative control (Fig. 3D).

### Expression and localization of Mpzl2 protein in the testes of wild-type and Cadm1-deficient mice

Using rat polyclonal antisera against mouse Mpzl2 polypeptide, we performed western-blot analysis of cell lysates obtained from the testes of adult wild-type and Cadm1-deficient mice (Fig. 4A, B). The immunoreactive band of 70 kDa representing Mpzl2 protein was detected in the testes of both wild-type and Cadm1-deficient mice. The intensity of this signal was about 2-fold higher in Cadm1-deficient mice than in wild-type mice.

The histological features of the seminiferous tubules of Cadm1-deficient mice were first compared with those of wild-type mice in PAS-hematoxylin stained paraffin sections (Fig. 5A, B). In Cadm1-deficient mice, shedding of spermatids, particularly those later than step 7, into the seminiferous tubular lumen was prominent. The number of elongated spermatids (step 10 and later) was reduced substantially, and the remaining elongated spermatids were irregular in shape. In contrast, the earlier spermatogenic cells up to pachytene spermatocytes appeared intact.

To examine the cellular localization of Mpzl2 protein, we performed IHC in cryostat sections of the adult Cadm1-deficient and wild-type mouse testes (Fig. 6). In Cadm1-deficient mice, immunostaining for Mpzl2 was found in both the seminiferous tubules and interstitial tissue (Fig. 6A). However, the immunoreactivity in the interstitial tissue, presumably in Leydig cells, was non-specific, because replacement of the primary antibody with normal rat serum resulted in the same immunostaining (Fig. 6B). In the seminiferous tubules of Cadm1-deficient mice, the signal for Mpzl2 protein was localized to leptotene/zygotene through to early pachytene spermatocytes but was not detected in late pachytene spermatocytes through to elongated spermatids (Fig. 6C). In wild-type mice, the immunoreactive cell populations were the same as in Cadm1-deficient mice but the intensity of immunoreactivity was weaker (Fig. 6D). Double-immunofluorescence microscopy for Mpzl2 and Cadm1 in the seminiferous tubules of adult wild-type mice demonstrated that early spermatocytes express both Mpzl2 and Cadm1, whereas elongated spermatids express Cadm1 but not Mpzl2 (Fig. 7A, B, C).

## IV. Discussion

Mpzl2, originally identified in mouse thymus as epithelial V-like antigen1 (EVA1), is a membrane protein with 215 amino acid residues, consisting of a signal peptide, an extracellular domain with only one Ig-like loop, a transmembrane domain, and a short intracellular domain [7]. Mpzl2 belongs to the IGS and considered to perform homophilic interaction with the same molecule. In the adult
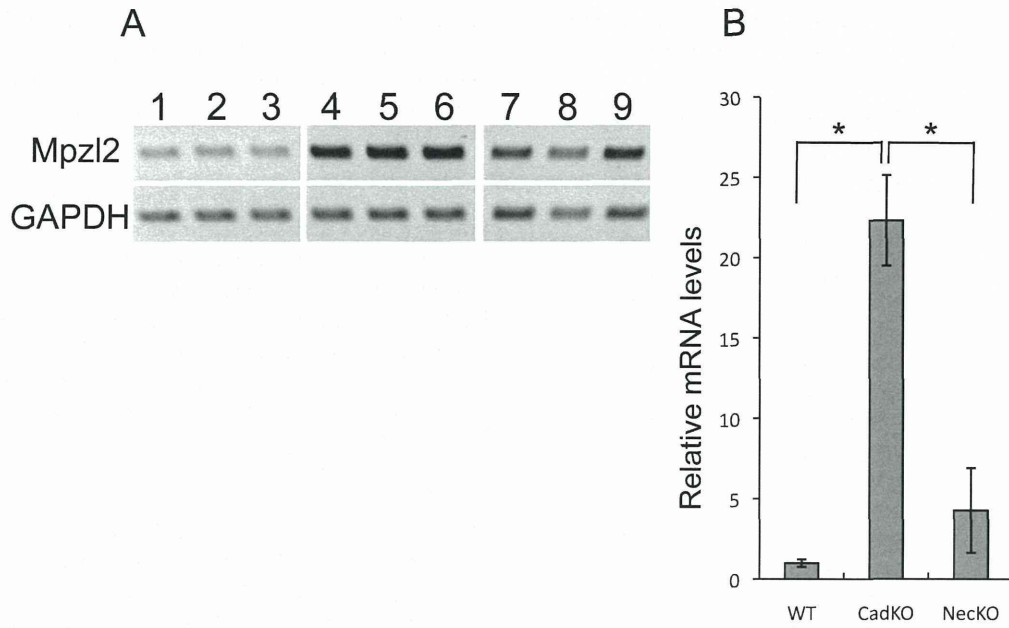
**Fig. 2.** (**A**) Conventional RT-PCR analysis showing the expression of Mpzl2 in the testes of wild-type (lanes1, 2, 3), Cadm1-deficient (4, 5, 6) and Nectin-3-deficient (7, 8, 9) adult mice. Amplified products from the total RNA of the testis were electrophoresed and stained with ethidium bromide. Expression of GAPDH is shown as positive control. (**B**) Realtime quantitative RT-PCR analysis showing the expression of Mpzl2 in the testes of wild-type (WT), Cadm1-deficient (CadKO) and Nectin-3-deficient (NecKO) adult mice. The relative levels of Mpzl2 mRNA adjusted with the corresponding levels of GAPDH mRNA are indicated. Each value represents mean±SD of 3 samples. *Significantly different ($P<0.01$).
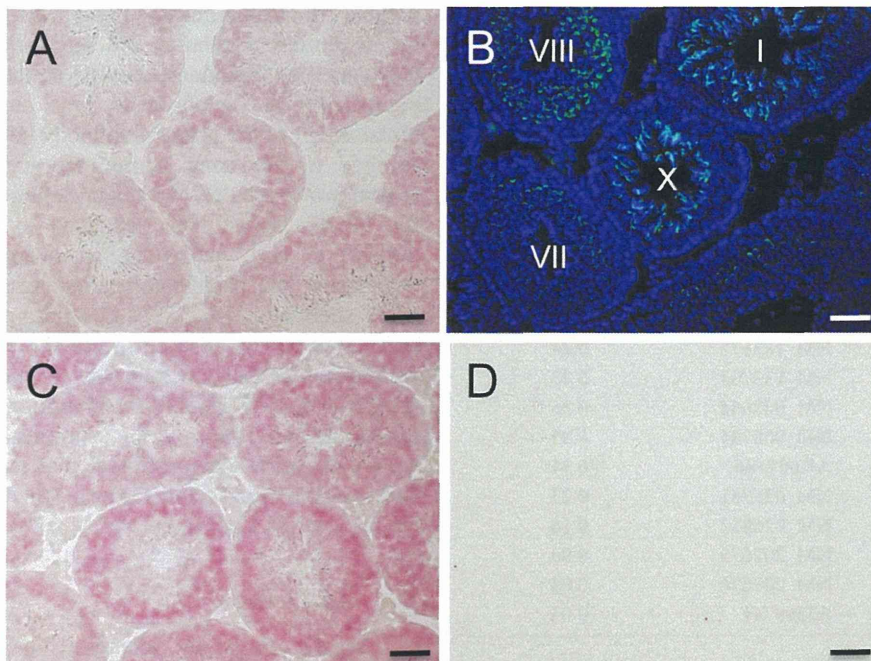


**Fig. 3.** (**A, C, D**) ISH analysis of the expression and localization of Mpzl2 mRNA in the testes of wild-type (**A, D**) and Cadm1-deficient (**C**) adult mice. Cryostat sections were hybridized with Dig-labeled antisense Mpzl2 probe in the absence (**A, C**) and presence (**D**) of excess unlabeled antisense probe, and the hybridization signal was visualized with alkaline-phosphatase histochemistry. (**B**) The same section as (**A**) was stained in the acrosomes with the PNA lectin histochemistry and in the nuclei with bisbenzimide. The spermatogenic stages of the seminiferous tubules are shown with roman numerals. Bar=50 μm.
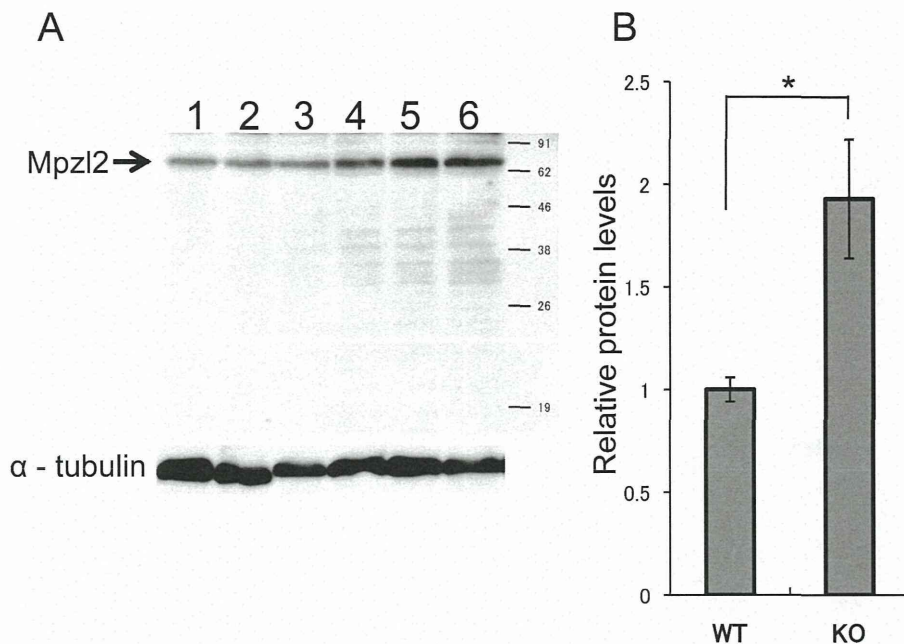
**Fig. 4.** Western blot analysis of the expression of Mpzl2 protein in the testes of wild-type (lanes 1, 2, 3) and Cadm1-deficient (4, 5, 6) adult mice. (**A**) The protein samples were electrophoresed, blotted and immunostained with rat anti-Mpzl2 antisera. For the control, staining with mouse anti-α-tubulin antibody was also performed. The molecular weight scale is shown. (**B**) The relative levels of Mpzl2 in the wild-type (WT) and Cadm1-deficient (KO) mice adjusted with the corresponding levels of α-tubulin. Each value represents mean±SD of 3 samples. *Significantly different (*P*<0.01).
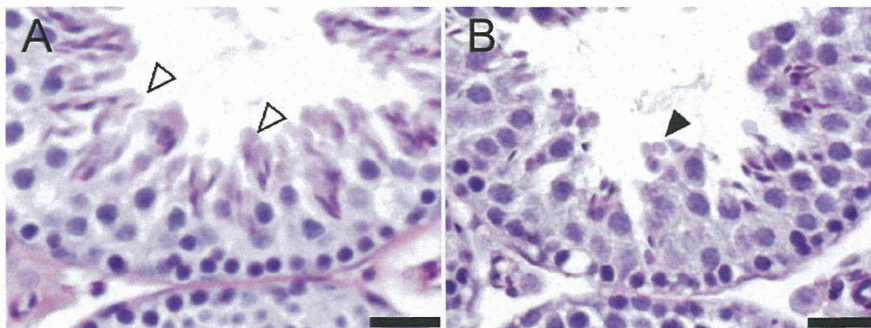


**Fig. 5.** Histological features of the seminiferous tubules of wild-type (**A**) and Cadm1-deficient (**B**) adult mice. Paraffin sections of the testes were stained with the PAS-hematoxylin method. Note that the elongated spermatids are lower in number and irregular in shape (black arrowhead) in Cadm1-deficient mouse, as compared with the normal step 12 elongated spermatids (white arrowheads) in wild-type mouse. Bar=50 μm.

mouse organs, Mpzl2 is expressed in the gut, kidney, liver, skin, testis, and thymus [7]. In the thymus, Mpzl2 is considered to be involved in the lymphocyte-stromal cell interaction, because it is expressed in thymocytes in the embryonic ages but in epithelial cells in the postnatal ages [4]. Transgenic mice overexpressing Mpzl2 in cortical epithelial cells of the thymus show increases in the size and absolute cell number of thymus, in spite of an increase of apoptosis in the thymus. Also, Mpzl2 is expressed in epithelial cells of the human choroid plexus and may play a role in the regulation of permeability in the choroid plexus

barrier [3]. So far, no report is available on the generation of the knock-out mouse for Mpzl2, thus it is unknown if Mpzl2 is indispensable for spermatogenesis.

In the present results, the levels of Mpzl2 mRNA increased by 20-fold and those of Mpzl2 protein increased by 2-fold in the testis from Cadm1-deficient mice compared with that from wild-type mice. Other cell adhesion molecules known to be expressed in spermatogenic cells, such as N-cadherin (N-cad), Coxsackievirus and adenovirus receptor (CAR), Jam-C, and Nectin-3 [27], were not detected among the 25-up-regulated genes in microarray. We also confirmed
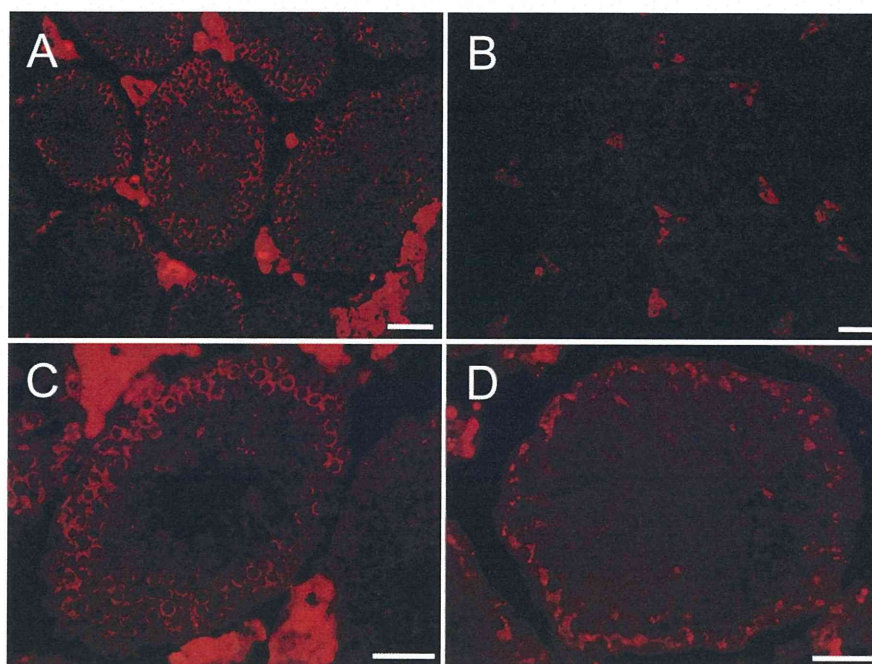
**Fig. 6.** Immunohistochemical localization of Mpzl2 in the testes of Cadm1-deficient (**A, B, C**) and wild-type (**D**) adult mice. Cryostat sections were immunostained with rat anti-Mpzl2 antisera (**A, C, D**) or non-immune rat serum (**B**). Note that the reactivity in the interstitial cells are detected without the primary antibody and thus is nonspecific. In both mice, Mpzl2-immunoreactivity is primarily localized in the earlier spermatogenic cells up to early pachytene spermatocytes. Bar=50 μm.
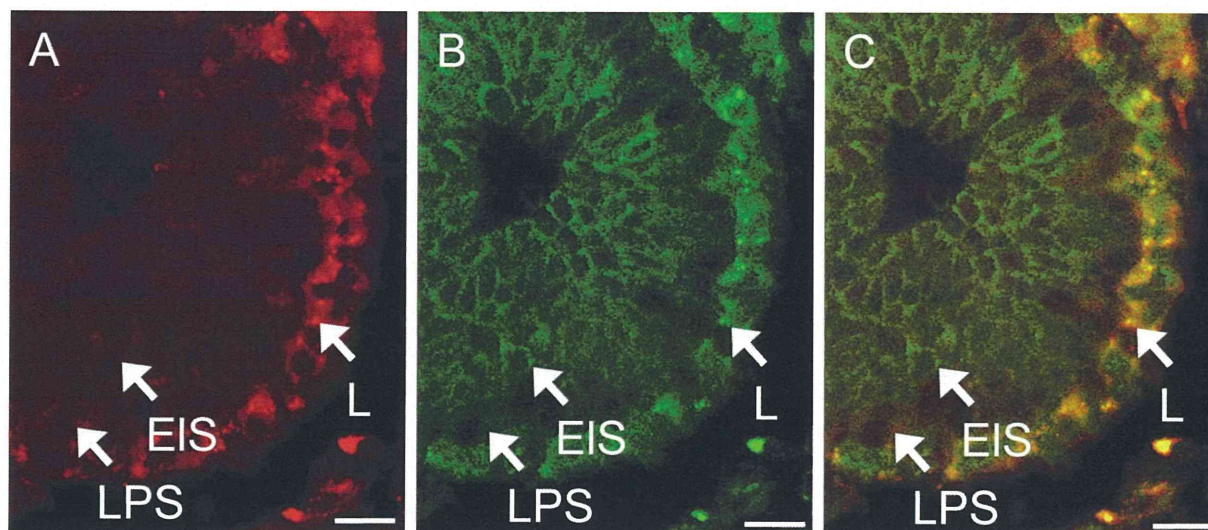


**Fig. 7.** Double immunostaining of the stage IX seminiferous tubule of a wild-type adult mouse with rat polyclonal anti-Mplz2 antisera and rabbit polyclonal anti-Cadm1 antibody. Note that in leptotene spermatocytes (L) the immunoreactivity for Mpzl2 (red, **A**) overlaps with that of Cadm1 antibody (green, **B**) when merged (yellow, **C**). In contrast, elongated spermatids (ElS) are immunopositive for Cadm1 but negative for Mpzl2, and late pachytene spermatocytes (LPS) are negative for both Mpzl2 and Cadm1. Bar=20 μm.

with RT-PCR that none of the mRNA for these adhesion molecules were increased in the testis from Cadm1-deficient mice (data not shown). Furthermore, Mpzl2 mRNA showed no increase in the testis from Nectin-3-deficient mice, which also has impaired spermatogenesis. Taken together, these results suggest that the upregulation of Mpzl2 expression in Cadm1-deficient mouse testis is a specific phenomenon. The precise mechanisms underlying this upregulation are unclear. Although both of the genes for Mpzl2 and Cadm1 are located on chromosome 9, their distance is as long as